The ARP2/3 complex prevents excessive formin activity during cytokinesis

Fung-Yi Chan[a,b], Ana M. Silva[a,b], Joana Saramago[a,b], Joana Pereira-Sousa[a,b], Hailey E. Brighton[c], Marisa Pereira[a,b], Karen Oegema[c], Reto Gassmann[a,b], and Ana Xavier Carvalho[a,b,*]

[a]Instituto de Investigação e Inovação em Saúde (i3S) and [b]Instituto de Biologia Molecular e Celular, Universidade do Porto, 4200-135 Porto, Portugal; [c]Department of Cellular and Molecular Medicine, Ludwig Institute for Cancer Research, University of California San Diego, La Jolla, CA 92093

ABSTRACT **Cytokinesis completes cell division by constriction of an actomyosin contractile ring that separates the two daughter cells. Here we use the early *Caenorhabditis elegans* embryo to explore how the actin filament network in the ring and the surrounding cortex is regulated by the single cytokinesis formin CYK-1 and the ARP2/3 complex, which nucleate nonbranched and branched filaments, respectively. We show that CYK-1 and the ARP2/3 complex are the predominant F-actin nucleators responsible for generating distinct cortical F-actin architectures and that depletion of either nucleator affects the kinetics of cytokinesis. CYK-1 is critical for normal F-actin levels in the contractile ring, and acute inhibition of CYK-1 after furrow ingression slows ring constriction rate, suggesting that CYK-1 activity is required throughout ring constriction. Surprisingly, although the ARP2/3 complex does not localize in the contractile ring, depletion of the ARP2 subunit or treatment with ARP2/3 complex inhibitor delays contractile ring formation and constriction. We present evidence that the delays are due to an excess in formin-nucleated cortical F-actin, suggesting that the ARP2/3 complex negatively regulates CYK-1 activity. We conclude that the kinetics of cytokinesis are modulated by interplay between the two major actin filament nucleators.**

Monitoring Editor
Francis A. Barr
University of Oxford

Received: Jul 7, 2018
Revised: Oct 23, 2018
Accepted: Nov 2, 2018

INTRODUCTION

Cytokinesis is the process that completes cell division by physically partitioning the contents of the mother cell into the two daughter cells. In metazoans, cytokinesis is accomplished via the assembly and constriction of a contractile ring, a differentiated part of the cell cortex that assembles around the cell equator beneath the plasma membrane after anaphase onset. Constriction of the ring progressively draws the plasma membrane inward, closing the gap between the two daughter cells. Electron microscopy studies show that the contractile ring is a thin layer primarily composed of circumferentially oriented actin filaments with interdigitating filaments of nonmuscle myosin II, integrated in a surrounding cortex that is mostly composed of a crisscross filamentous actin (F-actin) network (Schroeder, 1972; Sanger and Sanger, 1980; Maupin and Pollard, 1986; Kamasaki *et al.*, 2007; Henson *et al.*, 2017).

Formins are highly conserved multidomain proteins that dimerize through the formin-homology domain 2 to form a donut-shaped structure, which initiates actin filament assembly and remains associated with the barbed end of the actin filament to facilitate rapid elongation. Most formins exist in an autoinhibited conformation and are activated by binding to guanosine triphosphate (GTP)-bound Rho (Watanabe *et al.*, 1997; Otomo *et al.*, 2005; Rose *et al.*, 2005). Formins are required for cytokinesis in several species, including *Caenorhabditis elegans* (Chang *et al.*, 1997; Pelham and Chang, 2002; Severson *et al.*, 2002; Watanabe *et al.*, 2008). The current cytokinesis model postulates that formins are the nucleators/elongators of parallel actin filaments in the contractile ring (Severson *et al.*, 2002; Coffman *et al.*, 2013; Davies *et al.*, 2014) and are locally

This article was published online ahead of print in MBoC in Press (http://www.molbiolcell.org/cgi/doi/10.1091/mbc.E18-07-0471) on November 7, 2018.

Author contributions: A.X.C., R.G., K.O., and F.Y.C. conceived and designed experiments. A.X.C., R.G., and F.Y.C. wrote the manuscript. F.Y.C. and A.X.C. prepared the figures. F.Y.C., A.M.S., J.S., J.P.-S., H.E.B., and M.P. performed the experimental work and analyzed the data.

*Address correspondence to: Ana Xavier de Carvalho (anacarvalho@ibmc.up.pt).

Abbreviations used: ANOVA, analysis of variance; dsRNA, double-stranded RNA; F-actin, filamentous actin; GFP, green fluorescent protein; GTP, guanosine triphosphate; IPTG, isopropyl β-D-1-thiogalactopyranoside; NMY-2, nonmuscle myosin II.

activated by GTP-bound Rho at the cell equator (Motegi *et al.*, 2006; Watanabe *et al.*, 2010; Miller, 2011).

The ARP2/3 complex, another major F-actin nucleator, is composed of seven subunits, two of which, ARP2 and ARP3, closely resemble the structure of monomeric actin and serve as nucleation sites for new actin filaments. The complex binds to the sides of existing actin filaments and initiates growth of a new filament at a 70° angle from the mother filament, giving rise to branched actin filament networks (Pollard, 2007). During cytokinesis, it has been suggested that the ARP2/3 complex must be inactivated at the cell equator because it might otherwise interfere with the formin-nucleated F-actin network (Jordan and Canman, 2012; Pollard, 2017). Depletion of the ARP2/3 complex has been reported to result in cortical instability without altering the kinetics of cytokinesis (Severson *et al.*, 2002; Velarde *et al.*, 2007; Canman *et al.*, 2008; Loria *et al.*, 2012) and to facilitate cytokinesis in *C. elegans* embryos after inhibition of the Rho/Rac regulators ECT-2 or CYK-4 (*ect-2[ax751ts]* and *cyk-4[or749ts]*) (Canman *et al.*, 2008; Loria *et al.*, 2012). Formin and ARP2/3 complex-nucleated actin filament networks coexist in cells and therefore compete for a shared pool of monomeric actin (Burke *et al.*, 2014). How this competition impacts actin network homeostasis during cytokinesis, which heavily relies on actin network dynamics, is an emerging topic of investigation (Burke *et al.*, 2014; Suarez *et al.*, 2015). In this study, we use quantitative live-imaging in the *C. elegans* one-cell embryo to define the contributions of CYK-1 and the ARP2/3 complex to cortical F-actin organization and to the kinetics of cytokinesis. Our results reveal interplay between the ARP2/3 complex and CYK-1 and, contrary to prevailing models, suggest that the ARP2/3 complex makes a positive contribution to cytokinesis.

RESULTS

The ARP2/3 complex and CYK-1 nucleate the cortical actin filament network during cytokinesis

To dissect the roles of F-actin nucleators during cytokinesis in the *C. elegans* early embryo, we first sought to establish the identity of the nucleators that generate the cortical F-actin network. Live imaging of LifeAct::GFP (green fluorescent protein) revealed that during the early stages of cytokinesis in the one-cell embryo, F-actin is organized into a crisscross meshwork of filaments and bright puncta (Figure 1A). A similar organization had previously been observed with other probes for F-actin (Davies *et al.*, 2014; Ding *et al.*, 2017). We found that RNA interference (RNAi)-mediated codepletion of the formin CYK-1 and ARX-2, the ARP2 subunit of the ARP2/3 complex, greatly diminished cortical LifeAct::GFP signal and abolished both the filamentous and punctate actin population (Figure 1A). Thus, CYK-1 and the ARP2/3 complex are the main F-actin nucleators during cytokinesis in this system, consistent with a previous report (Davies *et al.*, 2014). To define the contribution of CYK-1 and the ARP2/3 complex to cortical F-actin organization, we analyzed single depletions of CYK-1 and ARX-2. Since thorough depletion of CYK-1 prevents cytokinesis (Supplemental Figure S1A; Severson *et al.*, 2002), we also examined partial CYK-1 depletions, which still allowed for completion of ring constriction. In control embryos, a distinct accumulation of linear and parallel actin filament bundles in a well-defined equatorial band was observed as the cortex started to deform (Figure 1B). Penetrant or partial depletion of CYK-1 led to the disappearance or substantial decrease of these F-actin bundles on the equatorial cortex, respectively (Figure 1B and Supplemental Figure S1A′), while the punctate actin structures were unaffected. By contrast, penetrant depletion of ARX-2, or treatment with the ARP2/3 complex inhibitor CK-666, resulted in complete loss of punctate structures, an accentuated crisscross meshwork, and a delay in the formation of a well-defined equatorial band (Figure 1B, Supplemental Figure S1B, and Supplemental Video S1). We conclude that CYK-1 and the ARP2/3 complex make distinct contributions to the organization of the cortical F-actin network during cytokinesis: CYK-1 is essential to generate F-actin bundles that form the contractile ring, while the ARP2/3 complex ensures the timely formation of the equatorial F-actin band.

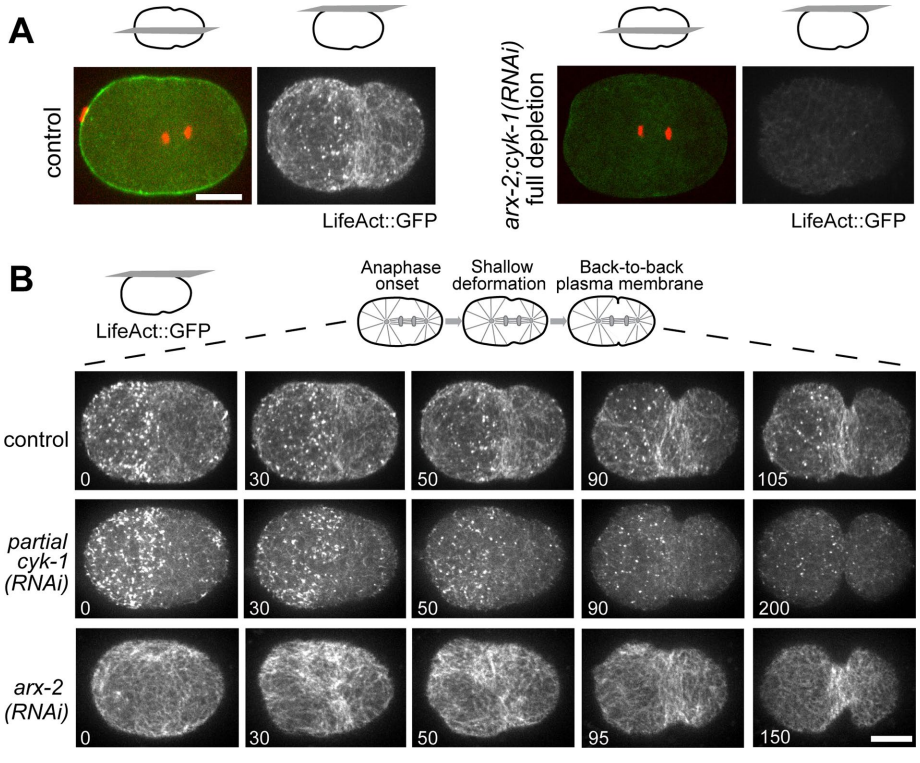

FIGURE 1: The ARP2/3 complex and the formin CYK-1 define the cortical actin filament network during cytokinesis in the one-cell *C. elegans* embryo. (A) Central and cortical sections of control embryos (left) or embryos codepleted of ARX-2 and CYK-1 (right) coexpressing LifeAct::GFP and mCherry::histone H2B (control $n = 9$; *arx-2; cyk-1(RNAi)* $n = 7$). (B) Stills from time-lapse imaging series showing the cortex of control, ARX-2–depleted, or CYK-1 partially depleted embryos expressing LifeAct::GFP. The interval shown is from anaphase onset (time point 0 s) to back-to-back membrane configuration (control $n = 9$; *arx-2(RNAi)* $n = 7$; *cyk-1(RNAi)* $n = 8$). Scale bars, 10 μm. See also Supplemental Figure S1.

CYK-1 is required for equatorial deformation and ring constriction

We next evaluated the contribution of CYK-1 and the ARP2/3 complex to three distinct stages of cytokinesis: 1) contractile ring assembly, defined as the interval between anaphase onset (i.e., the separation of sister chromatids) and shallow deformation at the equatorial cortex; 2) furrow initiation, defined as the interval between shallow deformation and formation of a

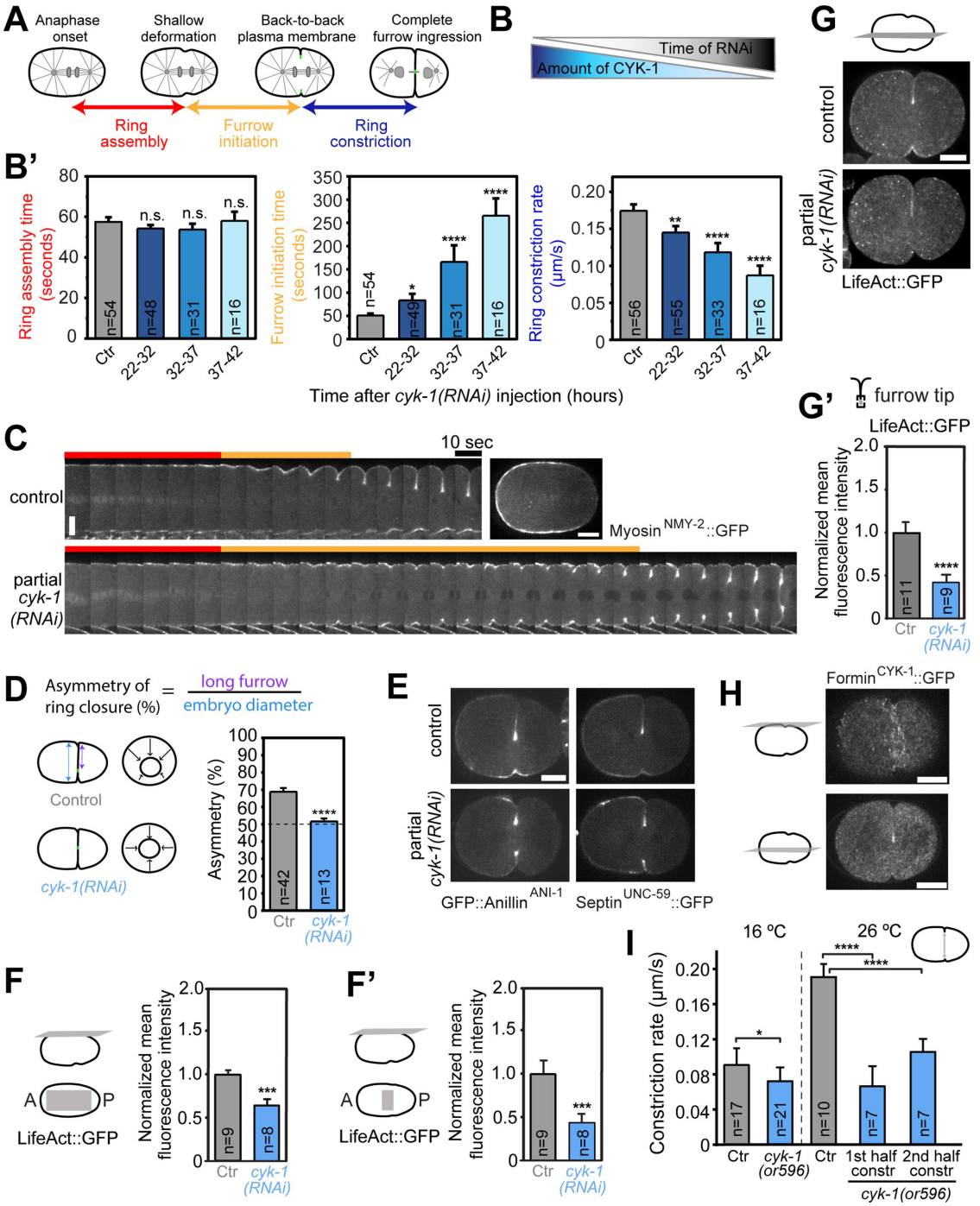

FIGURE 2: Partial depletion of CYK-1 impairs furrow initiation and slows down contractile ring constriction. (A) Schematic illustrating the intervals of contractile ring assembly, furrow initiation, and ring constriction in the one-cell embryo used for assessing the kinetics of cytokinesis. (B, B′) Mean duration of the cytokinesis intervals described in A measured in control embryos and embryos increasingly depleted of CYK-1 using an RNAi time-course regime (B). Embryos were imaged at defined time points after dsRNA injection—the longer the time after injection, the more depleted the embryos (B′). *N* is the number of embryos analyzed. Error bars represent 95% CI. (C) Kymographs of the equatorial region of control or CYK-1 partially depleted embryos expressing myosin^{NMY-2}::GFP. First frame corresponds to anaphase onset. Red and yellow bars indicate the intervals of ring assembly and furrow initiation, respectively. (D) Ring closure asymmetry (mean ± 95% CI) in control or CYK-1 partially depleted embryos measured after completion of ring constriction, as illustrated on the left. *N* is the number of embryos analyzed. (E) Central plane images of control or CYK-1 partially depleted embryos expressing GFP::anillin^{ANI-1} (left) and septin^{UNC-59}::GFP (right) at 50% furrow ingression (control GFP::anillin^{ANI-1} $n = 6$, septin^{UNC-59}::GFP $n = 7$; *cyk-1(RNAi)* GFP::anillin^{ANI-1} $n = 8$, septin^{UNC-59}::GFP $n = 6$). (F, F′) Mean LifeAct::GFP intensity (±95% CI) on the total cortex (F) or the equatorial region (F′) 10 s before shallow deformation. Values for *n* number of embryos were normalized to the mean of controls. (G, G′) Central plane images of control or CYK-1 partially depleted embryos expressing LifeAct::GFP at 50% furrow ingression (G) and average signal

back-to-back membrane configuration; and 3) ring constriction, defined as the interval after back-to-back membrane formation, when the furrow ingresses toward the embryo center and the contractile ring is observed at the furrow tip (Figure 2A). The timing of anaphase onset, equatorial shallow deformation, back-to-back membrane configuration, and the distance over time between both sides of the ingressing furrow (ring constriction rate) were determined in the central plane of the embryo. To define the role of CYK-1, we used an RNAi time course to progressively lower CYK-1 levels. We reasoned that if CYK-1 is responsible for generating the actin filaments that compose the contractile ring and the amount of F-actin in the ring in turn dictates constriction rate, rings containing progressively less formin should constrict at a correspondingly slower rate. The oocyte-producing gonad is ideally suited for RNAi time-course approaches: introduction of double-stranded RNA (dsRNA) by injection triggers the degradation of target mRNA in the syncytium while the existing target protein is continually packaged into oocytes. As a result, target protein levels in newly fertilized embryos gradually decrease with time after RNA injection (Kirkham *et al.*, 2003; Velarde *et al.*, 2007; Figure 2B). Live imaging of nonmuscle myosin$^{NMY\text{-}2}$::GFP showed that the ring assembly interval remained essentially constant despite the decrease in CYK-1 levels (57.6 ± 3.7 s vs. 58.1 ± 4 s in controls, Figure 2B′). By contrast, furrow initiation and ring constriction were increasingly affected. The furrow initiation interval increased approximately fivefold (265 ± 40 s vs. 52.7 ± 2.9 s in controls), and while control embryos steadily progressed from shallow U-shaped to steeper V-shaped equatorial deformation, embryos partially depleted of CYK-1 had difficulties in establishing the back-to-back membrane configuration, often making several abortive attempts (Figure 2C and Supplemental Video S2). In addition, ring constriction rate decreased by approximately twofold (0.08 ± 0.01 µm/s vs. 0.17 ± 0.01 µm/s in controls, Figure 2B′). Interestingly, CYK-1–depleted rings constricted concentrically within the division plane (Figure 2D). Concentric ring closure had previously been described for rings depleted of anillin or septins (Maddox *et al.*, 2007; Dorn *et al.*, 2016), yet both proteins were present at normal levels in CYK-1–depleted rings (Figure 2E). Thus, CYK-1 may promote asymmetric furrow ingression independently of anillin and septins.

Quantification of LifeAct::GFP intensity confirmed that partial depletion of CYK-1 (32–37 h postinjection) decreased F-actin levels in the cortex before furrow ingression (Figure 2F), especially in the equatorial region (Figure 2F′ and Supplemental Video S1). Levels of LifeAct::GFP were also decreased in the contractile ring at the tip of the ingressing furrow (Figure 2, G and G′, and Supplemental Video S3). Consistent with this, we observed that CYK-1::GFP in control embryos is enriched at the cell equator during shallow deformation and in the contractile ring during ring constriction (Figure 2H). Interestingly, a comparison of cytokinesis kinetics in one-, four-, and eight-cell embryos after partial CYK-1 depletion revealed that decreasing the levels of F-actin in the ring did not affect the previously reported scalability of contractile ring constriction rate (Carvalho *et al.*, 2009; Supplemental Figure S1C).

To ask whether ring constriction slowdown after partial *cyk-1(RNAi)* was a consequence of earlier problems during furrow initiation, we took advantage of the fast-acting *cyk-1(or596)* temperature-sensitive mutant (Davies *et al.*, 2014). Rapid upshifting to 26°C (the restrictive temperature of the mutant) in control one-cell embryos undergoing ring constriction resulted in faster constriction, as expected (Begasse *et al.*, 2015), whereas ring constriction in *cyk-1(or596)* failed to speed up when the upshift was performed immediately after formation of the back-to-back membrane configuration or during the second half of constriction (Figure 2I). We conclude that CYK-1 is essential for equatorial deformation and subsequently needs to remain active in the constricting ring to ensure normal constriction kinetics.

The ARP2/3 complex is required for timely assembly and constriction of the contractile ring

We next evaluated the role of the ARP2/3 complex, the other major actin filament nucleator during cytokinesis. ARX-2–depleted embryos presented slight cortical instability throughout cytokinesis (Supplemental Video S2; Loria *et al.*, 2012). Interestingly, we found that the kinetics of cytokinesis were significantly affected after penetrant depletion of ARX-2, as well as after treatment with the small molecule inhibitor CK-666 (Nolen *et al.*, 2009). Ring assembly was delayed (ARX-2 depletion 89.3 ± 8.5 s and CK-666 treatment 127.8 ± 20.2 s vs. 56.4 ± 2.6 s in controls), furrow initiation occurred faster (ARX-2 depletion 42 ± 3 s and CK-666 treatment 43.3 ± 5.6 s vs. 53.6 ± 2.5 s in controls), and ring constriction was slower (ARX-2 depletion 0.14 ± 0.01 µm/s and CK-666 treatment 0.14 ± 0.01 µm/s vs. 0.17 ± 0.01 µm/s in controls; Figure 3, A and B, and Supplemental Video S2). Ring closure was asymmetric like in controls (Figure 3C). Of note, ARX-2::GFP was not detected in the contractile ring but was diffusely present in the cytoplasm and in cortical puncta on the anterior side of control embryos (Figure 3D). Although a reduction of ARP2/3 complex levels might be expected at the cell equator (Yoshizaki *et al.*, 2003; Canman *et al.*, 2008; Zhuravlev *et al.*, 2017), we were unable to detect a difference in ARX-2::GFP signal at the equatorial cortex in the interval between anaphase onset and equatorial shallow deformation (Figure 3D′). We conclude that the ARP2/3 complex is important for timely cytokinesis and that its impact on cytokinesis kinetics is likely exerted from outside the contractile ring.

Delayed equatorial band formation after ARP2/3 complex depletion is unlikely due to altered distribution of polarity proteins

Depletion of ARX-2 resulted in a disorganized F-actin cortex and delayed the appearance of a well-defined equatorial band (Figures 1B and 4A). Anillin$^{ANI\text{-}1}$::GFP and nonmuscle myosin$^{NMY\text{-}2}$::GFP displayed similar cortical behaviors (Figure 4A). In contrast to controls, the equatorial band was only poorly defined in ARX-2–depleted embryos 50 s after anaphase onset and only became apparent later at the time of equatorial shallow deformation (Figure 4, A and B). ARX-2 depletion is known to affect the distribution of polarity

intensity (±95% CI) at the furrow tip for *n* number of embryos (G′), as indicated in the schematic. Values were normalized to the mean of controls. (H) Images of the cortical (60 s after anaphase onset) and center planes (at 50% furrow ingression) in control embryos expressing CYK-1::GFP ($n = 8$). (I) Ring constriction rate in one-cell control or *cyk-1(or596)* embryos at 16°C or after temperature upshift from 16° to 26°C during the first half or second half of constriction. Values are plotted as mean ± 95% CI for *n* number of embryos. Statistical significance was determined using one-way analysis of variance (ANOVA) followed by Bonferroni's multiple comparison test in B′ and I and the *t* test in D, F, F′, and G. *$p < 0.05$, **$p < 0.01$, ***$p < 0.001$, ****$p < 0.0001$, n.s. = not significant ($p > 0.05$). Scale bars, 10 µm.

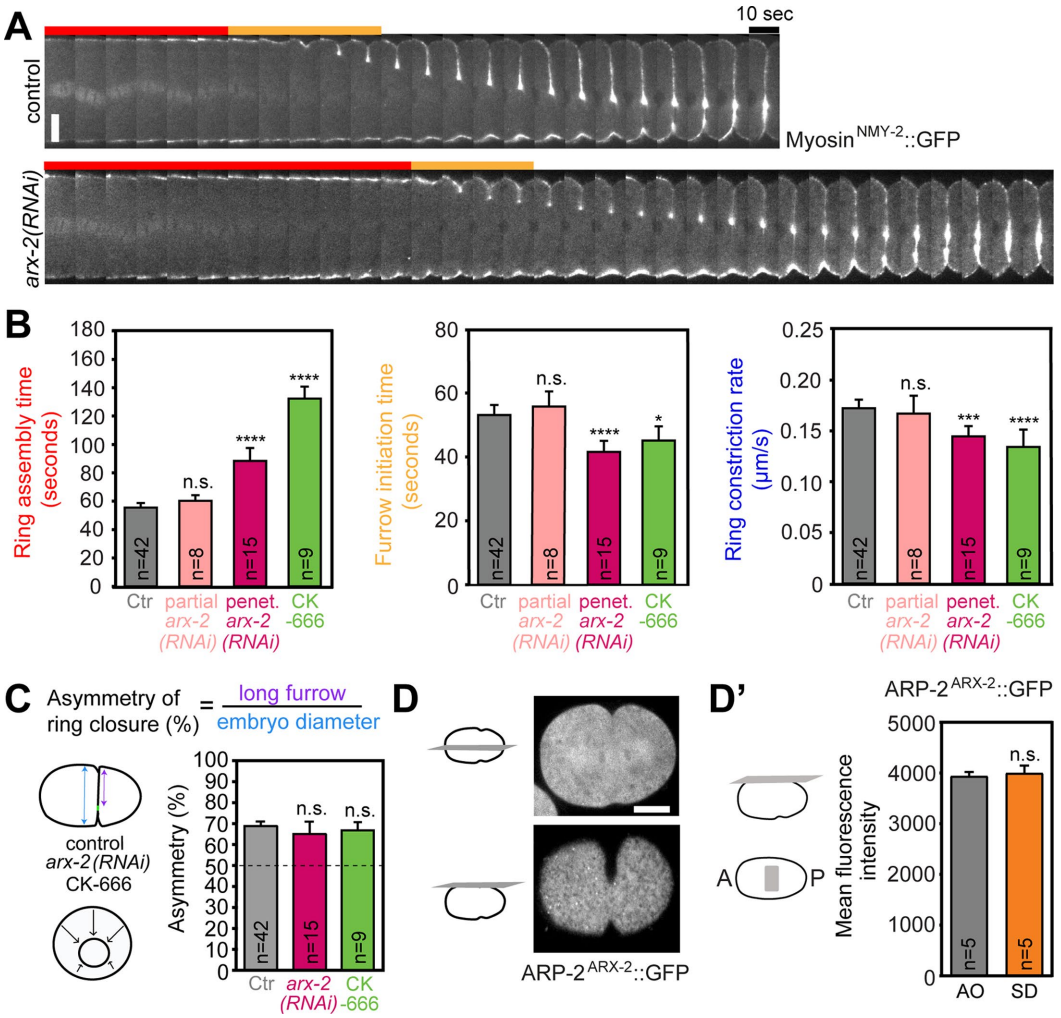

FIGURE 3: Inhibition of the ARP2/3 complex delays contractile ring assembly and slows down constriction. (A) Kymographs of the equatorial region in control or penetrant ARX-2–depleted one-cell embryos expressing myosin^{NMY-2}::GFP. First frame corresponds to anaphase onset. Red and yellow bars indicate the intervals of ring assembly and furrow initiation, respectively. (B) Mean duration (±95% CI) of ring assembly and furrow initiation, as defined in Figure 2A, and ring constriction rate in one-cell embryos for controls, partial, and penetrant (penet.) ARX-2 depletions, and after CK-666 treatment. Control values are derived from impermeable and permeable embryos, since they behaved similarly. *N* is the number of embryos analyzed. (C) Ring closure asymmetry (mean ±95% CI) in control embryos and after penetrant ARX-2 depletion or CK-666 treatment, measured after completion of ring constriction, as illustrated on the left. *N* is the number of embryos analyzed. (D) Central and cortical sections of embryos expressing ARP2^{ARX-2}::GFP at 120 s after anaphase onset. Images are representative of five embryos filmed. (D′) Mean intensity (± 95% CI) of ARP2^{ARX-2}::GFP on the equatorial cortex at anaphase onset (AO) and shallow deformation (SD). Statistical significance was determined using one-way ANOVA followed by Bonferroni's multiple comparison test, *$p < 0.05$, ***$p < 0.001$, ****$p < 0.0001$, n.s. = not significant ($p > 0.05$). Scale bars, 10 µm.

proteins before cytokinetic furrowing (Xiong *et al.*, 2011; Shivas and Skop, 2012), and cell polarity is thought to promote robust cytokinesis in *C. elegans* embryos (Xiong *et al.*, 2011; Shivas and Skop, 2012; Jordan *et al.*, 2016). It was therefore possible that equatorial band formation after ARX-2 depletion was delayed due to the effect on polarity. In control embryos, the polarity proteins PAR-6 and PAR-2 occupy the anterior and posterior halves of the cortex, respectively, with the boundary between the two domains situated at 55% of embryo length, where the furrow forms (Figure 4B). We confirmed that ARX-2–depleted embryos have a smaller PAR-6 domain and a correspondingly expanded PAR-2 domain (Figure 4B). The altered PAR-6/PAR-2 distribution was apparent at anaphase onset but was subsequently corrected, so that the PAR-6/PAR-2 domain boundary coincided with the furrow position by the time a back-to-back membrane configuration had formed (Supplemental Figure S2). Repositioning of the polarity boundary to match the cytokinesis furrow had been reported previously (Schenk *et al.*, 2010). Importantly, a similar alteration of PAR-6/PAR-2 distribution with subsequent correction occurred in embryos partially depleted of CYK-1, yet these embryos presented a well-defined equatorial band that formed with normal timing (Figure 4B). Thus, the delay in equatorial band formation in ARX-2–depleted embryos is unlikely to be caused by altered polarity protein distribution before furrow initiation.

ARP2/3 complex depletion increases CYK-1 and F-actin levels at the cell cortex and in the contractile ring

Measurements of fluorescence intensity on the cell cortex 50 s after anaphase onset and in the contractile ring at 50% ingression showed

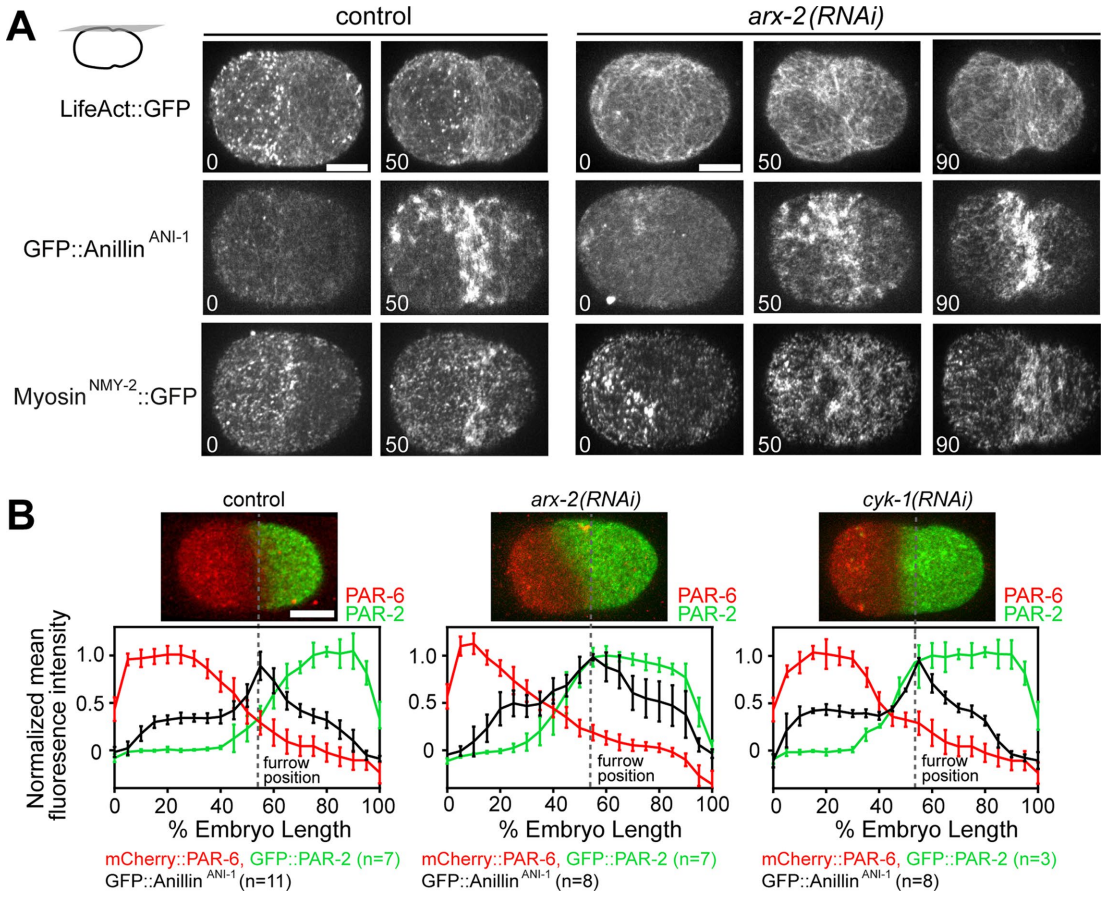

FIGURE 4: Delayed equatorial band formation after ARP2/3 complex inhibition is unlikely due to altered distribution of polarity proteins. (A) Cortical plane images of control (left) or ARX-2–depleted (right) embryos expressing LifeAct::GFP, GFP::anillin^{ANI-1} or myosin^{NMY-2}::GFP at the indicated times after anaphase onset (AO) (control LifeAct::GFP $n = 9$, GFP::anillin^{ANI-1} $n = 11$, myosin^{NMY-2}::GFP $n = 7$; *arx-2(RNAi)* LifeAct::GFP $n = 7$, GFP::anillin^{ANI-1} $n = 8$, myosin^{NMY-2}::GFP $n = 10$). (B) Cortical plane images of control, ARX-2–depleted, or CYK-1 partially depleted embryos coexpressing GFP::PAR-2 and mCherry::PAR-6 at 50 s after anaphase onset (top row). Mean fluorescence intensity (±95% CI) of cortical GFP::PAR-2 (green), mCherry::PAR-6 (red) and GFP::anillin^{ANI-1} (black) along the length of control (left), ARX-2–depleted (middle), or CYK-1 partially depleted (right) embryos, measured at 50 s after anaphase onset (bottom row). Values from *n* number of embryos were normalized to the maximum mean signal in controls. Dashed line indicates the furrow position. Scale bars, 10 µm. See also Supplemental Figures S2, S3, and S4.

that LifeAct::GFP levels were significantly increased after depletion of ARX-2 (Figure 5, A and B, Supplemental Figure S3, A–C, and Supplemental Videos S1 and S3). By contrast, cytoplasmic LifeAct::GFP levels remained unchanged relative to controls. Because monomeric actin distributes among competing actin filament networks (Burke *et al.*, 2014; Henson *et al.*, 2015), the increase in LifeAct::GFP levels after ARP2/3 complex depletion could be due to the excess of monomeric actin available for incorporation into existing formin-nucleated filaments, which would consequently become longer. Alternatively, elevated F-actin levels may reflect an increase in the number of nucleated filaments. Furthermore, as anillin has been described to suppress F-actin levels in the contractile ring (Jordan *et al.*, 2016), it is possible that the F-actin level increase observed in ARX-2–depleted embryos is a consequence of decreased anillin levels. We found that depletion of ARX-2 did not alter the amount of anillin in the contractile ring (Supplemental Figure S3, A–C) but resulted in a significant increase in CYK-1::GFP levels on the cortex (Supplemental Video S4) and at the tip of the ingressing furrow (Figure 5, C–F). A slight increase in the levels of GFP::AHPH (the C-terminus of anillin), a sensor for Rho activity, but not non-muscle myosin^{NMY-2}::GFP, a downstream target of Rho, were also observed (Supplemental Figure S3, A–D). To control for the effects of ARX-2 depletion on polarity, we abrogated polarity by depleting PAR-6, which did not increase cortical levels of LifeAct::GFP or CYK-1::GFP (Supplemental Figure S4, B and C). Taken together, these results suggest that ARP2/3 complex inhibition results in an increase in CYK-1 activity, which in turn increases the number of actin filaments on the cortex and in the constricting contractile ring.

Defects in cytokinesis kinetics after ARP2/3 depletion are rescued by codepletion of CYK-1

To test whether increased CYK-1 activity was responsible for the altered cytokinesis kinetics we observed when the ARP2/3 complex was inhibited, we performed double depletions of CYK-1 and ARX-2. In these experiments, ARX-2 was penetrantly depleted, as in previous experiments, whereas CYK-1 was partially depleted (Figure 6). The *cyk-1(RNAi)* condition was milder than the conditions used for the experiments in Figure 2B′ and on its own did not alter cytokinesis kinetics (see *Materials and Methods*; Figure 6B). Reverse-transcription PCR and immunoblotting confirmed that ARX-2 was

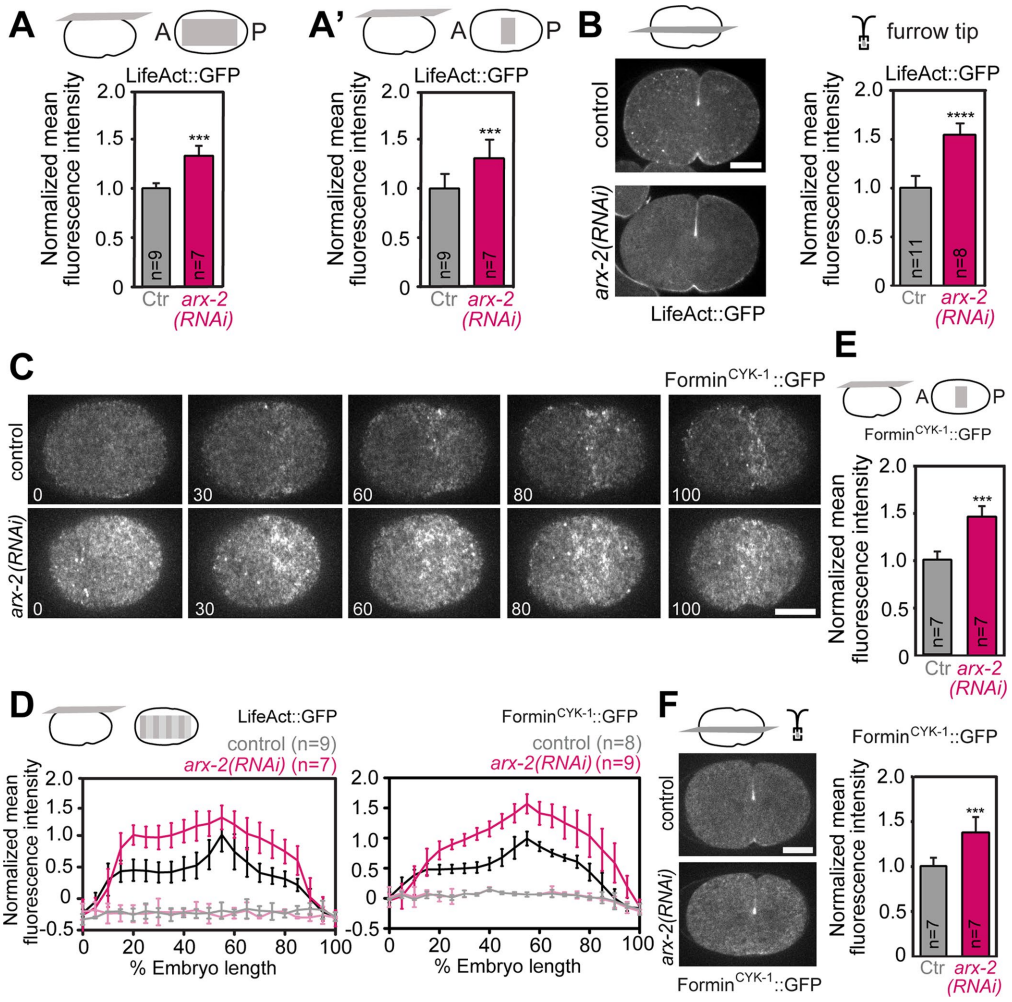

FIGURE 5: ARP2/3 complex inhibition increases F-actin and CYK-1 levels at the cell cortex and in the contractile ring. (A, A') Mean intensity (±95% CI) of LifeAct::GFP on the entire cortex (A) or the cortical equatorial region (A') 10 s before shallow deformation. Values from *n* number of embryos were normalized to the mean of controls. (B) Central plane images of control or ARX-2–depleted embryos expressing LifeAct::GFP at 50% furrow ingression (left) and mean signal intensity (±95% CI) at the furrow tip for *n* number of embryos (right), measured as indicated in the schematic. Values were normalized to the mean of controls. (C) Stills from time-lapse imaging series of the cortex in control or ARX-2–depleted embryos expressing formin^{CYK-1}::GFP from anaphase onset (time point 0 s) to back-to-back membrane formation (control $n = 11$; *arx-2(RNAi)* $n = 11$). (D) Mean fluorescence intensity (±95% CI) of cortical and cytoplasmic LifeAct::GFP (left) or formin^{CYK-1}::GFP (right) along the length of control or ARX-2–depleted embryos, measured at 50 s after anaphase onset. Cytoplasmic values are in light gray (control) and light pink (ARX-2 depletion). Values from *n* number of embryos were normalized to the maximum mean signal in controls. Difference in signal intensity of cortical LifeAct::GFP or formin^{CYK-1}::GFP between control and ARX-2–depleted embryos is statistically significant (***$p = 0.0009$ for LifeAct::GFP and ***$p = 0.0004$ for formin^{CYK-1}::GFP). (E) Mean intensity (±95% CI) of formin^{CYK-1}::GFP on the cortical equatorial region 10 s before shallow deformation. Values from *n* number of embryos were normalized to the mean of controls. (F) Central plane images of control or ARX-2–depleted embryos expressing formin^{CYK-1}::GFP at 50% furrow ingression (left) and mean signal intensity (±95% CI) at the furrow tip for *n* number of embryos (right), measured as indicated in the schematic. Values were normalized to the mean of controls. Statistical significance was determined using the *t* test in A, B, E, and F (***$p < 0.001$, ****$p < 0.0001$) and the grouped analysis two-way ANOVA followed by Bonferroni's multiple comparison test in D. Scale bars, 10 µm. See also Supplemental Figures S3 and S4.

depleted with similar efficiency in single and double depletions (Supplemental Figure S5). Codepletion of CYK-1 and ARX-2 rescued the increased F-actin levels in the constricting ring observed after ARX-2 single depletions (Figure 6C) but did not rescue the slight cortical instability caused by ARX-2 depletions. Strikingly, the abnormal timing for ring assembly and furrow initiation observed after ARX-2 depletion was rescued in codepleted embryos (ring assembly: ARX-2 depletion 94.5 ± 10.5 s, mild CYK-1 depletion 57 ± 5 s, and double depletion 61.3 ± 4.3 s vs. control 56.4 ± 2.8 s; furrow initiation: ARX-2 depletion 43 ± 2.8 s, mild CYK-1 depletion 52.3 ± 2.4 s, and double depletion 57.5 ± 7.3 s vs. control 53.6 ± 1.6 s, Figure 6, A and B). The ring constriction rate was also faster in the double depletion compared with ARX-2 depletion on its own, although it was not fully rescued (ARX-2 depletion 0.14 ± 0.01 µm/s, mild CYK-1 depletion 0.17 ± 0.04 µm/s, double depletion 0.15 ± 0.01 µm/s, control 0.17 ± 0.01 µm/s). Abrogation of polarity via

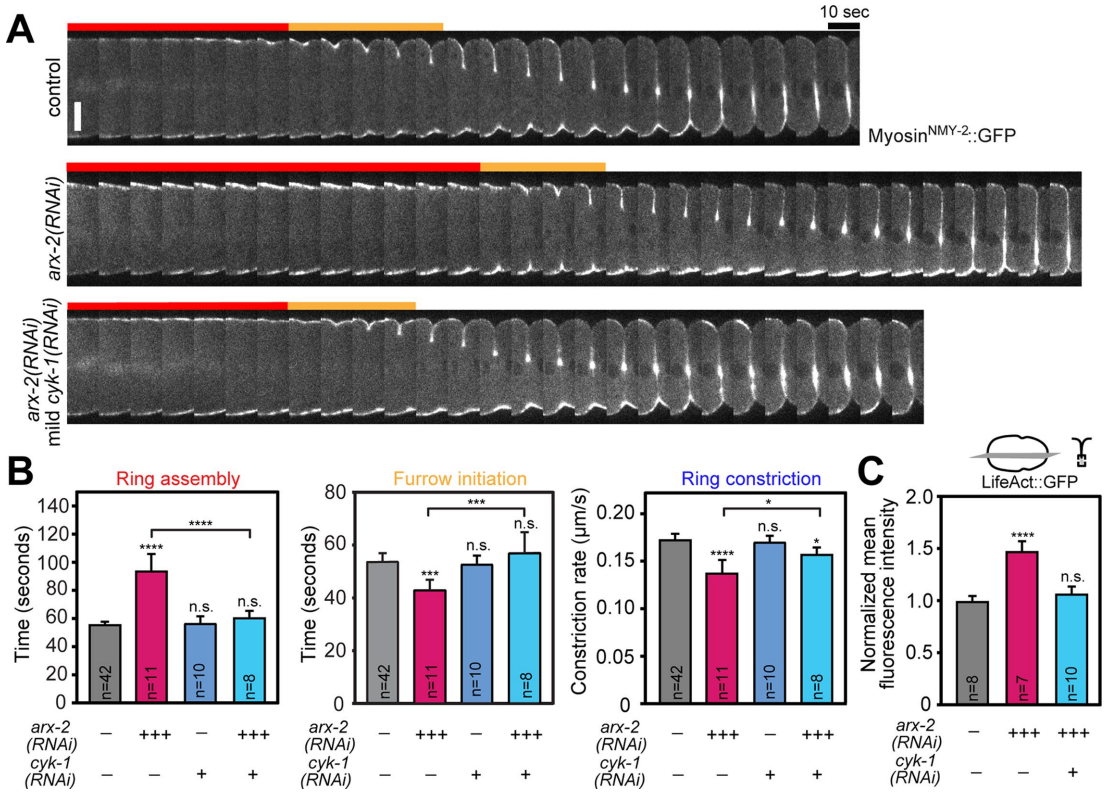

FIGURE 6: Delays in cytokinesis after ARP2/3 complex inhibition are caused by excess CYK-1 activity. (A) Kymographs of the equatorial region (myosin^{NMY-2}::GFP) in a control one-cell embryo and after depletion of ARX-2 or codepletion of ARX-2 and CYK-1. First frame corresponds to anaphase onset. Red and yellow bars indicate the intervals of ring assembly and furrow initiation, respectively. Scale bar, 10 µm. (B) Mean duration (±95% CI) of ring assembly and furrow initiation, as defined in Figure 2A, and ring constriction rate in one-cell embryos for the indicated conditions. ARX-2 depletions were penetrant (+++), while CYK-1 depletions were mild (+). *N* is the number of embryos analyzed. (C) Mean intensity (±95% CI) of LifeAct::GFP at 50% furrow ingression, measured as indicated in the schematic. Values were normalized to the mean of controls and RNAi conditions are as in B. *N* is the number of embryos analyzed. Statistical significance was determined using one-way ANOVA followed by Bonferroni's multiple comparison test; *$p < 0.05$, ***$p < 0.001$, ****$p < 0.0001$, n.s. = not significant ($p > 0.05$). See also Supplemental Figures S4 and S5.

par-6(RNAi) resulted in a delay in ring assembly but did not affect the timing of furrow initiation or ring constriction rate (Supplemental Figure S4, A and D). Importantly, delayed ring assembly after *par-6(RNAi)* failed to be rescued by CYK-1 codepletion (Supplemental Figure S4D), further supporting the idea that the effects of ARX-2 depletion on cytokinesis kinetics are not caused by altered polarity. We conclude that ARX-2 depletion changes the kinetics of cytokinesis primarily due to an increase in CYK-1 activity.

DISCUSSION

We identify the ARP2/3 complex and the formin CYK-1 as the predominant actin filament nucleators at the cell cortex of the dividing *C. elegans* one-cell embryo, in agreement with previous observations (Davies *et al.*, 2014). Using quantitative live-imaging approaches, we show that both the ARP2/3 complex and the formin CYK-1 positively contribute to the kinetics of contractile ring assembly, furrow initiation, and ring constriction. CYK-1 is known to be essential to elongate actin filaments that form the contractile ring (Severson *et al.*, 2002; Coffman *et al.*, 2013; Davies *et al.*, 2014), and, as expected, we find that decreasing CYK-1 levels reduces the amount of F-actin within the constricting ring. CYK-1 is enriched at the cell equator and in the constricting ring, and, in agreement with a specific role at the division plane, partial depletion of CYK-1 delays furrow initiation and slows ring constriction. Acute inactivation of CYK-1 after contractile ring assembly using the temperature-sensitive allele *or596* shows that slowed ring constriction is not simply a consequence of problems during furrow initiation. A previous study using the *or596* allele showed that inactivating CYK-1 during the second half of furrow ingression does not lead to cytokinesis failure (Davies *et al.*, 2014), raising the possibility that CYK-1 may become dispensable at later stages of cytokinesis. Our analysis of ring constriction rate reveals that inactivation of CYK-1 during the second half of furrow ingression causes a substantial slowdown of ring closure, suggesting that CYK-1 is active throughout cytokinesis. In vitro, formins have two distinct effects on actin filaments: they can efficiently elongate filaments when assisted by profilin, and they can cap filaments to prevent polymerization/depolymerization from the barbed end in the absence of profilin (Kovar *et al.*, 2003; Neidt *et al.*, 2008). The temperature-sensitive CYK-1 mutant encoded by allele *or596* is unable to polymerize F-actin in vitro and in vivo (Davies *et al.*, 2014), but its ability to cap actin filaments has not been examined. Actin polymerization is thought to occur within the contractile ring throughout cytokinesis (Silva *et al.*, 2016; Chew *et al.*, 2017) and could be formin dependent. However, it is also possible that CYK-1 acts as an F-actin nucleator/elongator during

early furrowing but subsequently transitions into a capper during ring constriction. In support of this idea, the elongation activity of cdc12p, the equivalent formin in *Schizosaccharomyces pombe*, is inhibited by myosin pulling on formin-bound actin filaments (Zimmermann *et al.*, 2017).

Current models postulate that the ARP2/3 complex acts exclusively as a negative regulator of cytokinesis (Canman *et al.*, 2008; Loria *et al.*, 2012; Zhuravlev *et al.*, 2017). By contrast, our results reveal that inhibition of the ARP2/3 complex delays contractile ring assembly and slows constriction, suggesting that the ARP2/3 complex makes a positive contribution. We show that the slowing of cytokinesis after ARP2/3 complex inhibition is caused by an increase in CYK-1-mediated actin polymerization on the cell cortex and in the contractile ring and not by altered polarity. This reveals regulatory cross-talk between the two main F-actin nucleators. Competition between CYK-1 and the ARP2/3 complex for the same pool of actin monomers, profilin-actin, and other factors capable of binding both nucleators could explain the increase in cortical F-actin levels when ARP2/3 activity is inhibited (Burke *et al.*, 2014; Suarez *et al.*, 2015). Importantly, we also observe that cortical levels of CYK-1 itself increase under these conditions. This suggests that ARP2/3 complex inhibition not only frees up monomeric actin that can be used by CYK-1 but also up-regulates CYK-1 activity. Increased monomeric actin levels after low-dose latrunculin B treatment were previously suggested to activate formins in *Xenopus* XTC cells, although this effect still depended on upstream Rho activity (Higashida *et al.*, 2008; Ramabhadran *et al.*, 2013). It is conceivable that ARP2/3 complex inhibition could activate CYK-1 by stimulating Rho activity, as ARX-2–depleted embryos have increased cortical levels of GFP::AHPH, a sensor for active Rho (Piekny and Glotzer, 2008; Tse *et al.*, 2012; Wagner and Glotzer, 2016). Increased Rho activity was also observed in ARP2/3 complex–depleted B35 rat neuroblastoma cells (Korobova and Svitkina, 2008). However, we note that the increased GFP::AHPH signal on the cell cortex is not as spread out as the signal of CYK-1::GFP or LifeAct::GFP, and overall levels of NMY-2::GFP and GFP::ANI-1, which also function downstream of Rho, are not increased after ARX-2 depletion. Thus, a potential effect of ARP2/3 complex inhibition on Rho will need further investigation with other sensors for Rho activity. Alternatively, the ARP2/3 complex could regulate CYK-1 through a direct interaction. For example, it has been proposed that a complex of mDia2 (one of the mammalian Diaphanous formins), WAVE2 (an ARP2/3 activator), and the ARP2/3 complex inhibits filopodial extension in HeLa cells (Beli *et al.*, 2008).

While our results suggest that the ARP2/3 complex is required in the surrounding cortex to prevent excessive CYK-1 activity, it is likely that the ARP2/3 complex is inactivated specifically at the cell equator to prevent interference with the formation of nonbranched actin filaments necessary for efficient filament sliding and ring closure. Branched filaments nucleated by the ARP2/3 complex increase drag, and filament entanglement by branches prevents efficient sliding and meshwork contraction (Reymann *et al.*, 2012; Yang *et al.*, 2012). Inhibition of ARP2/3 complex activity at the cell equator would be in agreement with the idea that the small GTPase Rac1, which acts upstream of the ARP2/3 complex in the lamellipodium (Pollard, 2007), is inactivated by the central spindle-localized GTPase-activating protein (GAP), MgcRacGAP^{CYK-4} (Canman *et al.*, 2008; Zhuravlev *et al.*, 2017), and that Rac1 activity is decreased at the division plane in HeLa cells (Yoshizaki *et al.*, 2003). Together, ARP2/3 complex-dependent down-regulation of formin activity in the surrounding cortex and inactivation of the ARP2/3 complex at the cell equator could reinforce the spatial segregation of branched and nonbranched actin filament networks during cytokinesis.

MATERIALS AND METHODS

Caenorhabditis elegans strains

Strains used in this study are listed in Supplemental Table S1 and were maintained on nematode growth medium (NGM) plates seeded with OP50 *Escherichia coli*. GCP374 strain was grown at 16°C; all other strains were grown at 20°C.

RNA interference

RNAi was performed either by feeding worms with HT115 *E. coli* bacteria that expressed the dsRNA of interest or by directly injecting worms with the dsRNA of interest. For production of dsRNA for worm injection against arx-2_RNA#1 or cyk-1_RNA#1 or par-6, oligonucleotides containing T7 or T3 promoter sequences (Supplemental Table S2) were used to amplify the corresponding regions from N2 cDNA and the PCR product was used as template for T3 or T7 transcription reactions (MEGAscript Transcription Kit; ThermoFischer Scientific). Transcription reactions were cleaned up (NucleoSpin RNA Clean-up, Macherey-Nagel) and diluted with 3× soaking buffer (32.7 mM Na_2HPO_4, 16.5 mM KH_2PO_4, 6.3 mM NaCl, and 14.1 mM NH_4Cl). For feeding RNAi of arx-2_RNA#2, cyk-1_RNA#2 or perm-1 (Supplemental Table S2), corresponding L4440 vectors were obtained from the Ahringer library (Source Bioscience) and sequenced to confirm gene target. Feeding RNAi plates were prepared as previously reported (Silva *et al.*, 2016).

Partial and penetrant depletions of ARX-2 were performed by injecting L4 worms and incubating them for 32–36 h (Figure 3B) and 45–48 h (Figures 1B, 3, A–C, 4, A and B, and 5 and Supplemental Figures S1C, S2, S3, and S4) at 20°C, respectively. Partial depletion of CYK-1 was performed by injecting cyk-1_RNAi#1 in L4 worms for 22–42 h (Figure 2B′) and for 32–37 h (Figure 2, C–G, Supplemental Figure S1C) at 16°C. For penetrant codepletion of ARX-2 and CYK-1 in Figure 1A, a mix of arx-2_RNAi#1 and cyk-1_RNAi#1 (0.5 µg/µl final concentration each) was injected in L4 worms and worms were incubated for 48 h at 20°C. To achieve the combination of penetrant ARX-2 depletion with mild CYK-1 depletion (Figure 6, A–C), L4 worms were subject to feeding RNAi with a mix of bacteria expressing arx-2_RNAi#2 and empty vector L4440 (mixing ratio 1:1) for 26–28 h at 20°C. Worms were then washed with M9 medium (86 mM NaCl, 42 mM Na_2HPO_4, 22 mM KH_2PO_4, and 1 mM $MgSO_4$), transferred to fresh NGM plates with a mix of bacteria expressing arx-2_RNAi#2 and cyk-1_RNAi#2 (ratio 1:1), and further incubated at 20°C for 20–22 h. For mild CYK-1 depletion alone, L4 worms were subject to feeding RNAi with bacteria expressing empty vector L4440 for 26–28 h at 20°C, transferred to a plate with a mix of bacteria expressing cyk-1_RNAi#2 and empty vector L4440 (ratio 1:1) and further incubated at 20°C for 20-22 h. We note that the level of CYK-1 depletion accomplished with this condition is milder than that obtained after injecting L4s with cyk-1_RNAi#1 for 22-32 h in Figure 2B′. For penetrant depletion of PAR-6, L4 worms were injected with dsRNA against par-6 and incubated for 52 h at 20°C (Supplemental Figure S4). To combine penetrant depletion of PAR-6 with mild depletion of CYK-1 (Supplemental Figure S4D), L4 worms were injected and incubated for 30–32 h at 20°C. Worms were then washed with M9 medium and transferred to fresh NGM plates with a mix of bacteria expressing cyk-1_RNAi#2 and empty vector L4440 (ratio 1:1) and further incubated at 20°C for 20–22 h.

Rapid temperature shifting during imaging

Rapid temperature shifts were performed using the CherryTemp fast heater-cooler system for microscopy (Cherry Biotech) that is coupled to a spinning-disk confocal system. This system was used to rapidly shift the temperature during live imaging of one-cell embryos expressing *cyk-1(or596)* temperature-sensitive mutant, myosin^{NMY-2}::GFP and mCherry::H2B (strain GCP374). In Figure 2I, temperature was shifted from 16°C (permissive temperature) to 26°C (restrictive) during the first half of ring constriction (ring diameter larger than 15 µm in one-cell embryos) or second half of ring constriction (ring diameter lower than 15 µm in one-cell embryos). Controls were wild-type embryos, expressing myosin^{NMY-2}::GFP and mCherry::H2B (strain GCP113) and subject to the same temperature conditions.

Drug treatments

Acute drug treatments were performed in permeabilized *C. elegans* embryos. To obtain permeabilized embryos, perm-1 RNAi conditions were optimized as suggested by Carvalho *et al.* (2011). In brief, 25–30 L4 worms were placed on a plate containing 0.005 mM isopropyl β-D-1-thiogalactopyranoside (IPTG) and HT115 *E. coli* bacteria expressing RNA against perm-1 were left at 20°C for 14–18 h. Worms were dissected and embryos filmed in meiosis medium (25 mM HEPES, pH 7.4, 5 mg/ml insulin, 20% heat-inactivated fetal bovine serum, and 60% Leibowitz-15 medium); 100 µM CK-666 (Sigma) was added at metaphase. At the end of each video, medium containing 33 µM FM4-64 (Molecular Probes) was added to the chamber to confirm that the imaged embryo was permeable.

Live imaging

Gravid hermaphrodites were dissected and one-cell *C. elegans* embryos were mounted on 2% agarose pads in a drop of M9 medium. Live imaging of embryos undergoing cytokinesis was performed at 20°C. Images were acquired on a spinning disk confocal system (Andor Revolution XD Confocal System; Andor Technology) with a confocal scanner unit (CSU-22; Yokogawa) mounted on an inverted microscope (Ti-E, Nikon) equipped with a 60× 1.42 oil-immersion Plan-Apochromat objective and solid-state lasers of 488 nm (250 mW) and 561 nm (250 mW). For image acquisition an electron multiplication back-thinned charge-coupled device camera (iXon; Andor Technology) was used. Acquisition parameters, shutters, and focus were controlled by Andor iQ3 software. For imaging of the center of one-cell embryos, 6 × 1–µm z-stacks and 2 × 1–µm z-stacks were collected in the 488- and 561-nm channels, respectively, every 10 s. For cortical imaging in one-cell embryos, 7 × 0.5–µm z-stacks were collected in the 488-nm channel every 5 s. These videos also included the acquisition of one central section of the embryo in the 488- or 561-nm channels. To monitor ring constriction in dividing cells of four- and eight-cell embryos (Supplemental Figure 1C), 11 × 1.0–µm z-stacks were collected in the 488-nm channel every 10 s. In all cases, except for imaging of ARX-2::GFP, exposure times were 100 ms for 488nm and 561-nm channels. Exposure time used to image embryos expressing ARX-2::GFP (Figure 3, D and D′) was 300 ms.

Cytokinesis kinetics

Measurements of time of ring assembly and furrow initiation, as well as overall ring constriction rate were performed in dividing one-cell embryos of the strain GCP9 (Figures 2B′, 3B, and 6B and Supplemental Figure 4, A and D). Time of ring assembly was the time interval between anaphase onset and the establishment of a shallow deformation in the equatorial region. Furrow initiation corresponded to the time interval between the establishment of the shallow deformation and the time when the plasma membranes of the nascent daughter cells became juxtaposed to one another. During ring constriction, the distance between the two sides of the ring on the z-plane where this was the widest was measured for each time point and plotted against time. The timing of anaphase onset, equatorial shallow deformation, back-to-back membrane configuration, and the distance over time between both sides of the ingressing furrow were determined in the central plane of the embryo. Ring constriction rate was the slope of the linear region between ~60 and 30% ingression. To determine initial ring perimeter and ring constriction rate in one-, four- and eight-cell embryos, we proceeded as described in Carvalho *et al.* (2009) (Supplemental Figure 1C). Analysis in the one-cell embryo was done as above, and ring perimeter was calculated from ring diameter (perimeter = diameter*π). In four- and eight-cell embryos, the perimeter of rings that constricted parallel to the imaging plane was measured over time. In these cases, ring perimeter was determined by manually tracing the ring outline in maximum intensity projections of z-stacks using the segmented line tool in Fiji. For all divisions, the mean initial cell perimeter was the perimeter around the cell equator immediately prior to the onset of detectable constriction.

Ring closure asymmetry

Asymmetry of ring closure was assessed by dividing the length of the longer side of the furrow by the diameter of the embryo just after completion of ring constriction (Figures 2D and 3C).

Fluorescence intensity measurements

To quantify the levels of Lifeact::GFP, formin^{CYK-1}::GFP, myosin^{NMY-2}::GFP, GFP::anillin^{ANI-1}, and GFP::AHPH$^{ANI-1_AHPH}$ at the tip of the cytokinetic furrow in one-cell embryos, the mean fluorescence intensity in a 7-pixel-wide, 21-pixel-long (1.3 × 3.7 µm) box drawn over the tip of the furrow at 50% ingression was measured and the mean cytoplasm signal on the anterior side of the embryo was subtracted (Figures 2G′, 5, B and F, and 6C and Supplemental Figure 3C). To quantify the levels of Lifeact::GFP, formin^{CYK-1}::GFP, myosin^{NMY-2}::GFP, GFP::anillin^{ANI-1}, ARP2^{ARX-2}::GFP, and GFP::AHPH$^{ANI-1_AHPH}$ at the cortical equatorial band in one-cell embryos, the mean fluorescence intensity within a 41-pixel-wide, 156-pixel-long (5.7 × 21.6 µm) box drawn over the cell equator (50–60% embryo length) was measured in maximum z-projections, and the mean cytoplasm signal on the anterior side of the embryo was subtracted (Figures 2F′, 3D′, 5, A′ and E, and Supplemental Figure 3B). The mean fluorescence intensities at the furrow tip and cortex were normalized to those of controls. For quantification of cortical and cytoplasm LifeAct::GFP, formin^{CYK-1}::GFP, myosin^{NMY-2}::GFP, GFP::anillin^{ANI-1}, GFP::AHPH$^{ANI-1_AHPH}$, GFP::PAR-2, and mCherry::PAR-6 along the embryo length in Figures 4B and 5D and Supplemental Figure S3A, a 90-pixel-wide line (approximately half the embryo width) was drawn and divided into 20 equal length segments from anterior (0%) to posterior (100%) in maximum z-projections at 50 s after anaphase onset. Mean fluorescence intensity was determined for each of the segments after cytoplasmic background subtraction. The values for each data set were normalized to the maximum intensity of controls.

Image analysis and statistics

All measurements and image processing were done using Fiji (ImageJ; National Institutes of Health) (Schindelin *et al.*, 2012). Z-stacks were projected using the maximum intensity projection tool (Figures 1, 2H, 3D, 4, A and B, and 5C and Supplemental Figures S1, A′, B, and C, S2, S3D, and S4, A and C). Images within each panel were scaled equally. The equatorial region of the central plane was

selected to create the kymographs shown in Figures 2C, 3A, and 6A and Supplemental S1A using the Make Montage tool. Graph plotting, linear regressions, and statistical analyses were performed with Prism 7.0 (GraphPad Software). All error bars represent the 95% confidence interval (CI) of the mean.

ACKNOWLEDGMENTS

The research leading to these results has received funding from the European Research Council under the European Union's Horizon 2020 research and innovation program to A.X.C. (grant agreement 640553, ACTOMYO) and under the European Union's Seventh Framework program (FP7/2007-2013) to R.G. (grant agreement ERC-2013-StG-338410-DYNEINOME). Funding was also provided by the project Norte-01-0145-FEDER-000029–Advancing Cancer Research: From basic knowledge to application, supported by the Norte Portugal Regional Operational Programme (NORTE 2020), under the PORTUGAL 2020 Partnership Agreement, through the European Regional Development Fund (FEDER). A.X.C. and R.G. have FCT Investigator positions funded by FCT and cofunded by the European Social Fund through Programa Operacional Temático Potencial Type 4.2 promotion of scientific employment (IF/00901/2013/CP1157/CT0001 to A.X.C. and IF/01015/2013/CP1157/CT0006 to R.G.). F.Y.C. and A.M.S. hold FCT postdoctoral fellowships SFRH/BPD/93528/2013 and SFRH/BPD/95707/2013, respectively.

REFERENCES

Begasse M, Leaver M, Vazquez F, Grill S, Hyman A (2015). Temperature dependence of cell division timing accounts for a shift in the thermal limits of C. áelegans and C. ábriggsae. Cell Rep 10, 647–653.

Beli P, Mascheroni D, Xu D, Innocenti M (2008). WAVE and Arp2/3 jointly inhibit filopodium formation by entering into a complex with mDia2. Nat Cell Biol 10, 849–857.

Burke TA, Christensen JR, Barone E, Suarez C, Sirotkin V, Kovar DR (2014). Homeostatic actin cytoskeleton networks are regulated by assembly factor competition for monomers. Curr Biol 24, 579–585.

Canman JC, Lewellyn L, Laband K, Smerdon SJ, Desai A, Bowerman B, Oegema K (2008). Inhibition of Rac by the GAP activity of centralspindlin is essential for cytokinesis. Science 322, 1543–1546.

Carvalho A, Desai A, Oegema K (2009). Structural memory in the contractile ring makes the duration of cytokinesis independent of cell size. Cell 137, 926–937.

Carvalho A, Olson SK, Gutierrez E, Zhang K, Noble LB, Zanin E, Desai A, Groisman A, Oegema K (2011). Acute drug treatment in the early C. elegans embryo. PLoS One 6, e24656.

Chang F, Drubin D, Nurse P (1997). cdc12p, a protein required for cytokinesis in fission yeast, is a component of the cell division ring and interacts with profilin. J Cell Biol 137, 169–182.

Chew TG, Huang J, Palani S, Sommese R, Kamnev A, Hatano T, Gu Y, Oliferenko S, Sivaramakrishnan S, Balasubramanian MK (2017). Actin turnover maintains actin filament homeostasis during cytokinetic ring contraction. J Cell Biol 216, 2657–2667.

Coffman VC, Sees JA, Kovar DR, Wu J-Q (2013). The formins Cdc12 and For3 cooperate during contractile ring assembly in cytokinesis. J Cell Biol 203, 101–114.

Davies T, Jordan SN, Chand V, Sees JA, Laband K, Carvalho AX, Shirasu-Hiza M, Kovar DR, Dumont J, Canman JC (2014). High-resolution temporal analysis reveals a functional timeline for the molecular regulation of cytokinesis. Dev Cell 30, 209–223.

Ding WY, Ong HT, Hara Y, Wongsantichon J, Toyama Y, Robinson RC, Nédélec F, Zaidel-Bar R (2017). Plastin increases cortical connectivity to facilitate robust polarization and timely cytokinesis. J Cell Biol 216, 1371–1386.

Dorn JF, Zhang L, Phi T-T, Lacroix B, Maddox PS, Liu J, Maddox AS (2016). A theoretical model of cytokinesis implicates feedback between membrane curvature and cytoskeletal organization in asymmetric cytokinetic furrowing. Mol Biol Cell 27, 1286–1299.

Henson JH, Ditzler CE, Germain A, Irwin PM, Vogt ET, Yang S, Wu X, Shuster CB (2017). The ultrastructural organization of actin and myosin II filaments in the contractile ring: new support for an old model of cytokinesis. Mol Biol Cell 28, 613–623.

Henson JH, Yeterian M, Weeks RM, Medrano AE, Brown BL, Geist HL, Pais MD, Oldenbourg R, Shuster CB (2015). Arp2/3 complex inhibition radically alters lamellipodial actin architecture, suspended cell shape, and the cell spreading process. Mol Biol Cell 26, 887–900.

Higashida C, Suetsugu S, Tsuji T, Monypenny J, Narumiya S, Watanabe N (2008). G-actin regulates rapid induction of actin nucleation by mDia1 to restore cellular actin polymers. J Cell Sci 121, 3403–3412.

Jordan SN, Canman JC (2012). Rho GTPases in animal cell cytokinesis: an occupation by the one percent. Cytoskeleton 69, 919–930.

Jordan SN, Davies T, Zhuravlev Y, Dumont J, Shirasu-Hiza M, Canman JC (2016). Cortical PAR polarity proteins promote robust cytokinesis during asymmetric cell division. J Cell Biol 212, 39–49.

Kamasaki T, Osumi M, Mabuchi I (2007). Three-dimensional arrangement of F-actin in the contractile ring of fission yeast. J Cell Biol 178, 765–771.

Kirkham M, Müller-Reichert T, Oegema K, Grill S, Hyman AA (2003). SAS-4 is a C. elegans centriolar protein that controls centrosome size. Cell 112, 575–587.

Korobova F, Svitkina T (2008). Arp2/3 complex is important for filopodia formation, growth cone motility, and neuritogenesis in neuronal cells. Mol Biol Cell 19, 1561–1574.

Kovar DR, Kuhn JR, Tichy AL, Pollard TD (2003). The fission yeast cytokinesis formin Cdc12p is a barbed end actin filament capping protein gated by profilin. J Cell Biol 161, 875–887.

Loria A, Longhini KM, Glotzer M (2012). The RhoGAP domain of CYK-4 has an essential role in RhoA activation. Curr Biol 22, 213–219.

Maddox AS, Lewellyn L, Desai A, Oegema K (2007). Anillin and the septins promote asymmetric ingression of the cytokinetic furrow. Dev Cell 12, 827–835.

Maupin P, Pollard TD (1986). Arrangement of actin filaments and myosin-like filaments in the contractile ring and of actin-like filaments in the mitotic spindle of dividing HeLa cells. J Ultrastruct Mol Struct Res 94, 92–103.

Miller AL (2011). The contractile ring. Curr Biol 21, R976–R978.

Motegi F, Velarde NV, Piano F, Sugimoto A (2006). Two phases of astral microtubule activity during cytokinesis in C. elegans embryos. Dev Cell 10, 509–520.

Neidt EM, Skau CT, Kovar DR (2008). The cytokinesis formins from the nematode worm and fission yeast differentially mediate actin filament assembly. J Biol Chem 283, 23872–23883.

Nolen BJ, Tomasevic N, Russell A, Pierce DW, Jia Z, Mccormick CD, Hartman J, Sakowicz R, Pollard TD (2009). Characterization of two classes of small molecule inhibitors of Arp2/3 complex. Nature 460, 1031–1034.

Otomo T, Tomchick DR, Otomo C, Panchal SC, Machius M, Rosen MK (2005). Structural basis of actin filament nucleation and processive capping by a formin homology 2 domain. Nature 433, 488–494.

Pelham RJ, Chang F (2002). Actin dynamics in the contractile ring during cytokinesis in fission yeast. Nature 419, 82–86.

Piekny AJ, Glotzer M (2008). Anillin is a scaffold protein that links RhoA, actin, and myosin during cytokinesis. Curr Biol 18, 30–36.

Pollard TD (2007). Regulation of actin filament assembly by Arp2/3 complex and formins. Annu Rev Biophys Biomol Struct 36, 451–477.

Pollard TD (2017). Nine unanswered questions about cytokinesis. J Cell Biol 216, 3007–3016.

Ramabhadran V, Hatch AL, and Higgs HN (2013). Actin monomers activate inverted formin 2 by competing with its autoinhibitory interaction. J Biol Chem 288, 26847–26855.

Reymann A-C, Boujemaa-Paterski R, Martiel J-L, Guérin C, Cao W, Chin HF, De La Cruz EM, Théry M, Blanchoin L (2012). Actin network architecture can determine myosin motor activity. Science 336, 1310–1314.

Rose R, Weyand M, Lammers M, Ishizaki T, Ahmadian MR, Wittinghofer A (2005). Structural and mechanistic insights into the interaction between Rho and mammalian Dia. Nature 435, 513–518.

Sanger JM, Sanger JW (1980). Banding and polarity of actin filaments in interphase and cleaving cells. J Cell Biol 86, 568–575.

Schenk C, Bringmann H, Hyman AA, Cowan CR (2010). Cortical domain correction repositions the polarity boundary to match the cytokinesis furrow in C. elegans embryos. Development 137, 1743–1753.

Schindelin J, *et al*. (2012). Fiji: an open-source platform for biological-image analysis. Nat Methods 9, 676–682.

Schroeder TE (1972). The contractile ring. II. Determining its brief existence, volumetric changes, and vital role in cleaving Arbacia eggs. J Cell Biol 53, 419–434.

Severson AF, Baillie DL, Bowerman B (2002). A Formin Homology protein and a profilin are required for cytokinesis and Arp2/3-independent assembly of cortical microfilaments in C. elegans. Curr Biol 12, 2066–2075.

Shivas JM, Skop AR (2012). Arp2/3 mediates early endosome dynamics necessary for the maintenance of PAR asymmetry in Caenorhabditis elegans. Mol Biol Cell 23, 1917–1927.
Silva AM, Osório DS, Pereira AJ, Maiato H, Pinto IM, Rubinstein B, Gassmann R, Telley IA, Carvalho AX (2016). Robust gap repair in the contractile ring ensures timely completion of cytokinesis. J Cell Biol 215, 789–799.
Suarez C, Carroll RT, Burke TA, Christensen JR, Bestul AJ, Sees JA, James ML, Sirotkin V, Kovar DR (2015). Profilin regulates F-actin network homeostasis by favoring formin over Arp2/3 complex. Dev Cell 32, 43–53.
Tse YC, Werner M, Longhini KM, Labbe J-C, Goldstein B, Glotzer M (2012). RhoA activation during polarization and cytokinesis of the early Caenorhabditis elegans embryo is differentially dependent on NOP-1 and CYK-4. Mol Biol Cell 23, 4020–4031.
Velarde N, Gunsalus KC, Piano F (2007). Diverse roles of actin in C. elegans early embryogenesis. BMC Dev Biol 7, 142.
Wagner E, Glotzer M (2016). Local RhoA activation induces cytokinetic furrows independent of spindle position and cell cycle stage. J Cell Biol 213, 641–649.
Watanabe N, Madaule P, Reid T, Ishizaki T, Watanabe G, Kakizuka A, Saito Y, Nakao K, Jockusch BM, Narumiya S (1997). p140mDia, a mammalian homolog of Drosophila diaphanous, is a target protein for Rho small GTPase and is a ligand for profilin. EMBO J 16, 3044–3056.
Watanabe S, Ando Y, Yasuda S, Hosoya H, Watanabe N, Ishizaki T, Narumiya S (2008). mDia2 induces the actin scaffold for the contractile ring and stabilizes its position during cytokinesis in NIH 3T3 cells. Mol Biol Cell 19, 2328–2338.
Watanabe S, Okawa K, Miki T, Sakamoto S, Morinaga T, Segawa K, Arakawa T, Kinoshita M, Ishizaki T, Narumiya S (2010). Rho and anillin-dependent control of mDia2 localization and function in cytokinesis. Mol Biol Cell 21, 3193–3204.
Xiong H, Mohler WA, Soto MC (2011). The branched actin nucleator Arp2/3 promotes nuclear migrations and cell polarity in the C. elegans zygote. Dev Biol 357, 356–369.
Yang Q, Zhang XF, Pollard TD, Forscher P (2012). Arp2/3 complex–dependent actin networks constrain myosin II function in driving retrograde actin flow. J Cell Biol 197, 939–956.
Yoshizaki H, Ohba Y, Kurokawa K, Itoh RE, Nakamura T, Mochizuki N, Nagashima K, Matsuda M (2003). Activity of Rho-family GTPases during cell division as visualized with FRET-based probes. J Cell Biol 162, 223–232.
Zhuravlev Y, Hirsch SM, Jordan SN, Dumont J, Shirasu-Hiza M, Canman JC (2017). CYK-4 regulates Rac, but not Rho, during cytokinesis. Mol Biol Cell 28, 1258–1270.
Zimmermann D, Homa KE, Hocky GM, Pollard LW, De La Cruz EM, Voth GA, Trybus KM, Kovar DR (2017). Mechanoregulated inhibition of formin facilitates contractile actomyosin ring assembly. Nat Commun 8, 703.